

BSc Thesis Chemical Science  
and Engineering

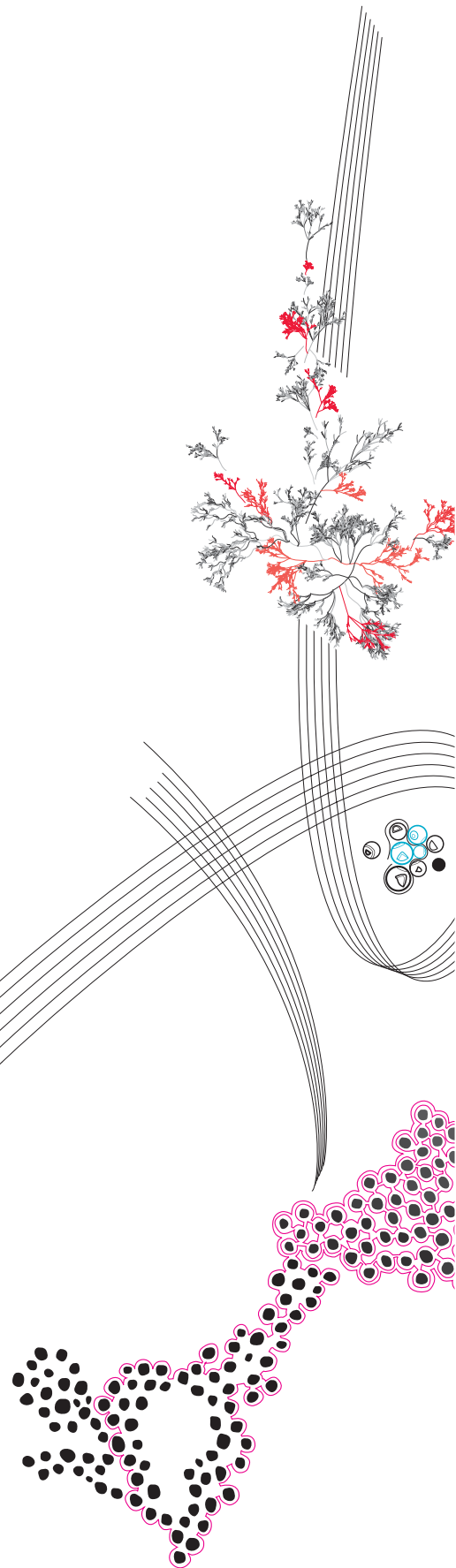
Electrospinning and  
characterization of  
 $ZrO_2$  nanofibers  
functionalized  
with palladium sites

Cazac Dan

Supervisor: Prof. Han Gardeniers  
Dr. Arturo Susarrey  
Jedrzej Winczewski MSC

July, 2022

Faculty of Science and Technology,  
Chemical Science and Engineering





# Electrospinning and characterization of ZrO<sub>2</sub> nanofibers functionalized with palladium sites

Cazac Dan\*

July, 2022

## Abstract

The support material often limits heterogeneous catalysis via mass transfer, diffusion, and consequentially reaction rates. To address this issue, the chemical industry often has to develop new ways to support a metal catalyst by introducing different structures and materials. One such structure are nanofibers due to their ability to minimize diffusion within the support material. This study presents a fabrication method of nanofibers made from a very underused material, such as zirconia, doped with palladium. The zirconia nanofibers or ZNFs prepared via the in-situ method, show a characteristic fiber structure ranging from 56 to 41 nm in average diameter. The prepared nanofibers, have been found to be in a mix of tetragonal and monoclinic phases, mainly tetragonal, with higher concentrations of monoclinic phase at the surface fibers. XPS and EDS have proved the presence of palladium sites on the surface of the fibers. Additionally, the palladium salt concentration was found to lower the average fiber's diameter, further aiding in increasing the surface-to-volume ratio.

---

\*Email: [d.cazac@student.utwente.nl](mailto:d.cazac@student.utwente.nl)

# Contents

<b>1</b>	<b>Introduction</b>	<b>4</b>
1.1	Electrospinning . . . . .	4
1.2	Thermal treatment . . . . .	5
1.3	Zirconium oxide nanofibers . . . . .	5
<b>2</b>	<b>Theoretical background</b>	<b>7</b>
2.1	Electrospinning . . . . .	7
2.1.1	Electrospinning solution . . . . .	8
2.1.2	Humidity . . . . .	8
2.1.3	Nozzle/Collector distance . . . . .	8
2.2	Characterization techniques . . . . .	8
2.2.1	XRD (X-Ray Diffraction Spectroscopy) . . . . .	8
2.2.2	Raman Spectroscopy . . . . .	8
2.2.3	SEM and EDS . . . . .	9
2.2.4	XPS (X-ray photoelectron spectroscopy) . . . . .	9
<b>3</b>	<b>Experimental Section</b>	<b>10</b>
3.1	Electrospinning of Pd doped ZrO <sub>2</sub> nanofibers . . . . .	10
3.2	Morphological characterization . . . . .	10
3.3	Spectroscopic characterization . . . . .	10
3.4	Structure characterization . . . . .	11
<b>4</b>	<b>Results and discussion</b>	<b>12</b>
4.1	X-ray Diffraction Spectroscopy . . . . .	12
4.2	Raman Spectroscopy . . . . .	14
4.3	X-ray photoelectron spectroscopy . . . . .	15
4.4	Morphological analysis . . . . .	16
4.4.1	EDS (Energy-dispersive X-ray spectroscopy) . . . . .	19
<b>5</b>	<b>Conclusions</b>	<b>20</b>
<b>6</b>	<b>Acknowledgments</b>	<b>21</b>
<b>A</b>	<b>Abbreviations</b>	<b>25</b>
<b>B</b>	<b>Palladium Oxide XRD</b>	<b>25</b>
<b>C</b>	<b>SEM</b>	<b>26</b>
<b>D</b>	<b>XPS</b>	<b>26</b>

## Abbreviations

NP	Nanoparticles
ZNF	Zirconium nanofibers
TCD	Nozzle to collector distance
XRD	X-ray diffraction spectroscopy
SEM	Scanning electron microscope
TEM	Transmission electron microscope
EDS	Energy dispersive X-ray spectroscopy
XPS	X-ray photoelectron spectroscopy
PVP	Polyvinylpyrrolidone

# 1 Introduction

The chemical industry is focused on the perpetual process of improvement of heterogeneous catalysts [1], since more efficient catalysis can lead to higher yields and lower energy requirements. The activity of a catalyst is highly dependent on the support material used. The support material can substantially influence the rate of the reaction and, in some cases, promote selectivity towards the product of the reaction. However, well-performing catalyst materials tend to be challenging to formulate, as they must fulfill several criteria, i.e., high surface area, good heat, mass transfer capabilities, ease of manufacturing, and have interaction with the catalyst that promote the reaction. Recent studies have proved that the increase in surface area [2] following a transition to nano-scale structures from micro-scale support material has led to a substantial increase in the activity of a catalyst by improving the diffusion and overall mass transport capabilities of the catalyst supporting material. To promote mass transport, homogeneous catalysis can be used as an alternative to the already established processes, e.g., palladium nanoparticles offer a high surface area to volume ratio [3] and a strong catalytic activity since mass transport limitations are a lot lower than in heterogeneous catalysis. However, NP's lack resistance to heat and are prone to aggregation. Thus a heterogeneous catalyst with properties similar to nanoparticles could be a better solution. One very promising category of support material for heterogeneous catalysts are nanofibers. The advantage of the nanofibers over other support materials is the diameter of the threads, which are in nanometric range. A small diameter results in a high surface area to volume ratio [2], which benefits the mass transport. Additionally, the fabrication of the fibers via electrospinning is a fairly easy process, once optimized, but with a disadvantage of being very time consuming.

## 1.1 Electrospinning

Nanofibers [4] can be prepared from different materials using various techniques, like in-situ polymerization, sol-gel synthesis, and low-temperature stirring. However, electrospinning is the most used and efficient approach because of its versatility and the possibility of combining it with other techniques for various fiber morphology. The electrospinning process is relatively straightforward. It consists of mainly three parts [4]: a nozzle connected to a pump containing a viscous polymeric precursor, a high voltage power supply, and a grounded collector with adjustable settings as can be seen in figure.1. Electrospinning [4] occurs through an electrohydrodynamic mechanism later described in the theoretical background. To fabricate the polymeric precursor, the matrix polymer is combined with metal salts, e.g., poly (vinyl pyrrolidone) (PVP) dissolved in a solvent. The metal-organic salts [5], act as the building material for the ceramic nanofiber since, after electrospinning, the fibers are thermally treated, and all the organic components are combusted in oxygen, substituting the organic ion from the salts with oxygen.

## 1.2 Thermal treatment

After the fibers have been produced, they are placed in a muffled furnace where the organic compounds are combusted in the air [5], and the metal particles get oxidized, annealing with each other, forming a ceramic nanofiber as can be seen in figure.1. The fiber crystal structure can be controlled via the oven temperature and sample residence time. In this academic work, the annealing process will be performed at 500°C with a temperature slope of 1°C/min for 8 hours and 40 minutes and then kept at 500°C for two hours.

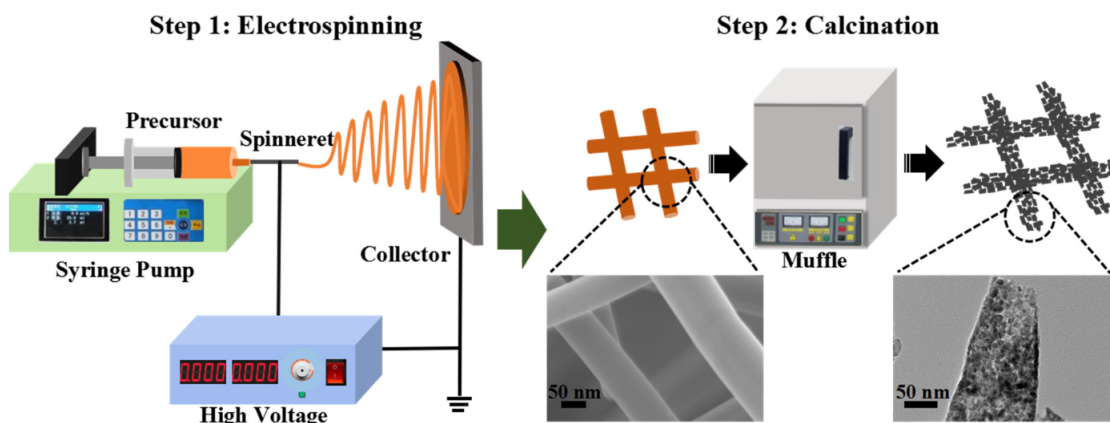


FIGURE 1: Electrospinning setup for nanofibers fabrication and their further calcination [6]

## 1.3 Zirconium oxide nanofibers

The application of nanofibers as support material is not a new topic. Multiple studies have been conducted to study the efficiency of different ceramic nanofibers support [7]-[8], e.g., Alumina-supported palladium doped nanofibers [8], with high efficiency for CO oxidation compared to conventional non-fiber support structures. Zirconia supported [5] palladium catalyst has been proven to have good chemical and thermal stability. Additionally, zirconium oxide has been demonstrated to increase the catalytic activity of the noble metals due to the presence of coordinatively unsaturated sites [9] on the surface of the support. These sites adsorb the reactive species preventing aggregation on the surface of the catalyst at high temperatures, thus stabilizing the donor sites. This further reinforces the idea that a combination of zirconium oxide nanofibers with palladium sites could perhaps be used as an efficient catalyst, e.g., CO oxidation as a model reaction [8].

Fabrication of Pd/ZrO<sub>2</sub> nanofibers is a straightforward process and is achieved by an in-situ growth of the Pd particles from the palladium acetate during the calcination of the nanofibers. While preparing the precursor (polymeric solution), zirconium salts will be combined with palladium salts for their further calcination and formation of Pd sites on the surface of zirconia. Unfortunately, with this method, only poor control over the amount of catalyst available on the nanofiber surface is possible. To mitigate this issue, the researchers at MCS (Mesoscale Chemical Systems) decided to try and deposit Pd particles of the support material via wet impregnation [10]. This will allow the researchers to study the catalyst concentration on the surface of the fibers for both preparation methods. Thus, this thesis will try to answer the following questions: “Does the palladium concentration of 0.5%, 1%, and 2% influence the morphology and structure of the zirconia fibers? Is the in-situ preparation method suitable for functionalizing the fibers with palladium sites? ”

This academic assignment will focus on preparing the Pd/ZrO<sub>2</sub> nanofibers via electrospinning and in-situ growth method. With their further analysis with XRD and Raman for an understanding of the crystal structure of the nanofibers, SEM, and XPS analysis for an understanding of the surface topology and the average fiber diameter. As a continuation, within a broader study, the activity of the samples of Pd/ZrO<sub>2</sub> nanofibers prepared via two different methods (in-situ and wet impregnation) will be analyzed for CO oxidation by our research partner (CONICET Argentina – National Scientific and Technical Research Council).

## 2 Theoretical background

This chapter will contain detailed information on the electrospinning of the nanofibers, followed by characterization techniques used to assess the palladium sites within the zirconia fibers.

### 2.1 Electrospinning

Electrospinning [1] is a relatively old fiber fabrication technique. Within the field, it is considered one of the most used techniques in nanofibers fabrication due to the versatility and ease of fiber production. Electrospinning is used to fabricate ceramic, composite, and polymer nanofibers. The technique can be used to create multiple assemblies of nanofibers, such as nanowires, nano-grooves, and nano-woven mesh [11]. Due to this high flexibility, electrospinning can be used for various in-situ assemblies, meaning high customizability of the fibers with multiple materials, such as Pd, for catalytic purposes. The most straightforward variation of the technique creates nanofibers via an electric field [12] that induces a charge on the surface of the viscoelastic solution at the end of the tube (fig.2). The solution's surface tension holds the material in place until the repulsion of charges creates a force directly opposite to the surface tension, resulting in a formation of a Taylor cone [13], which extends with the increase of the electric field. At one point, the extension of the cone reaches a critical level that breaks the surface tension of the solution, and a charged jet of solution from the tip of the Taylor cone is expelled to the metal collector plate, which acts as a counter electrode [14]. During its 'flight time,' the solvent evaporates, creating nano-scale fibers, which are then collected at the grounded plate. The fiber's morphology during electrospinning depends on multiple parameters, such as the composition of the precursor solution, the nozzle to collector distance, and the humidity of the air, solvent, concentration of polymer, and nozzle diameter.

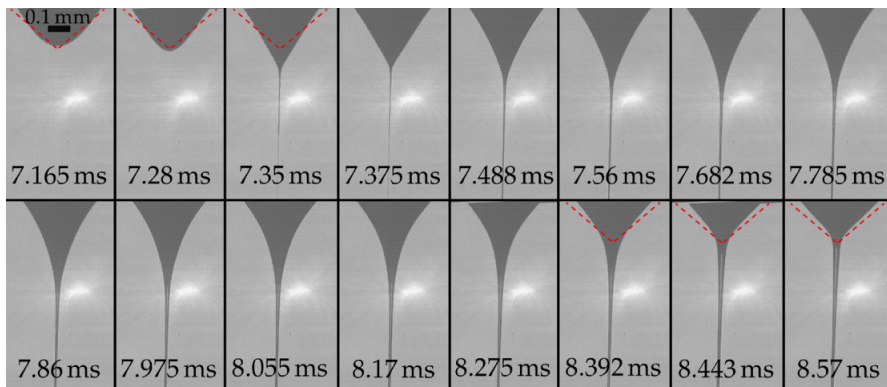


FIGURE 2: Formation of a Taylor cone [15]

### **2.1.1 Electrospinning solution**

Polymer solvent systems [14] are a critical parameter in the electrospinning process since the composition of the solvent and polymer can influence the process parameters, the formation of the Taylor cone, and the infusion speed. Different polymers interact differently with many solvents and salts, e.g., you cannot dissolve PAN in H<sub>2</sub>O. However, solvents can be used to customize the resulting fibers. For instance, using a PVA-Water system results in fibers in the range of 100-500 nm, a PVP-Ethanol/DMF [16] system, with some additional parameters, according to Yang et al.[14] resulted in fibers with a 20 nm diameter.

### **2.1.2 Humidity**

The humidity of the air plays an important role in the NF's fabrication[14]. Since the fibers are drying during the ejection process, a constant humidity level facilitates fibers formation and proper structure without beads formation. Thus, the less disturbance in temperature and humidity, the better the morphology of the fibers will be. Low humidity is undesirable since it can lead to the clogging of the nozzle.

### **2.1.3 Nozzle/Collector distance**

The electric field strength is very susceptible the nozzle to the collector distance (TCD). The fiber's diameter and bead formation are mainly influenced by the TCD[14]. Beads influence the morphology of the fibers by creating "islands" of polymer that break a continuous fiber. Generally, beads are considered an unfavorable outcome since it lowers the overall surface area available. Thus, TCD is one of the most critical parameters in the nanofibers or NF's fabrication since it has the strongest influence on the drying process.

## **2.2 Characterization techniques**

### **2.2.1 XRD (X-Ray Diffraction Spectroscopy)**

The crystal structure of the sample is studied using XRD. From the resulting diffractograms, it is possible to tell the phase of the material, and the grain size of the zirconium dioxide crystals using the Scherrer equation[17], the intensity of the peaks of different concentrations can be compared to establish if there are any major changes in grain size depending on the palladium concentration. XRD, however, is rather limited in terms of the palladium particle characterization since the peaks of spectra will inevitably overlap[18] with the tetragonal phase of zirconia.

### **2.2.2 Raman Spectroscopy**

Additionally, to XRD, Raman spectroscopy can be also used to determine the crystal structure of the material and serves as a complementary step to XRD.

### 2.2.3 SEM and EDS

Scanning electron microscope is used for the characterization of the surface morphology of the fibers. Conventional microscopy is impossible to use at the nanoscale due to limitations of light diffraction limit. Thus for the analysis of the size, but also surface morphology of the samples, SEM is implemented. Scanning the surface of the fibers with an electron beam allows for the characterization of the fabricated nanofibers at high magnifications using scattered electrons that hit a detector. The main interest of the thesis is assessing the quality and size of the palladium nanoparticles, the diameter of the fibers and their structure, as well as the uniformity of the fibers. SEM images can help detect flaws in the synthesis process, such as bead formation or sintering problems. It is the most potent technique used in this thesis that allows for accurate qualitative results. SEM will be combined with energy-dispersive x-ray spectroscopy [19] to determine the sample composition, homogeneity of the elemental distribution. This powerful analytical technique can analyze the energy emitted by the sample and create a map of X-ray emissions on top of the SEM image. Since every element has different emission patterns, the map can be used to study the abundance of palladium in the sample as well as its dispersity.

### 2.2.4 XPS (X-ray photoelectron spectroscopy)

XPS is used to study the elemental composition of the nanofibers as well as the oxidation state of the element. It is a powerful analytical technique that analyzes the material's surface resulting in exact elemental composition. Additionally, it can determine if the palladium is bonded to other elements. It is a highly accurate technique that can quantitatively assess the concentration of each element, allowing for a better understanding of the composition of the fibers as well as possible mistakes during the electrospinning process, like the detection of elements or features that shouldn't be a part of the fiber.

## 3 Experimental Section

### 3.1 Electrospinning of Pd doped ZrO<sub>2</sub> nanofibers

To prepare palladium doped zirconium nanofibers or Pd-ZNF, an uncommercial electrospinning system was used, constructed by the researchers at the University of Twente. The system allows to apply maximum parameters of 15 kV at the nozzle and -10 kV at the collector with a variable distance. The precursor was prepared by mixing 3.5% w/w of (Zirconium Acetylacetonate technical grade Sigma-Aldrich), 37.5% w/w of N, N-dimethylformamide (DMF), and 52% of ethanol (100% Technical grade, BOOM B.V., The Netherlands) to generate Zirconia nanofibers precursor. For a palladium source, Pd acetate (ACS, Sigma-Aldrich, 98% purity) was used. Three different Pd concentrations were prepared (0.00009%, 0.00018%, 0.00036% w/w) equivalent to (0.5, 1, 2 % w/w of Pd in ZrO<sub>2</sub>) mixed with the precursor in a sonic bath (Elmasonic P30H) at room temperature and a 37 kHz (80% power) for 15 minutes. 7% w/w polyvinylpyrrolidone (PVP, MW 1,300,000) was added to the mixture and sonicated for another 10 minutes to help dissolve the PVP.

The viscous precursor solution was spun in the aforementioned setup using a steel nozzle (Nordson Orange) with 0.65 mm outer and 0.33 mm inner diameter and an outer Polytetrafluoroethylene (PTFE) coating on the nozzle, to create a hydrophobic layer between the nozzle and the cathode. Precursor solution was transferred to a 12 ml (Luer lock) syringe and pumped with a syringe pump (PHD 2000). The setup ran with a tip to collector distance (TCD) of 16 cm, a potential of 15kV on the nozzle, and -9.5 kV on the collector. The infusion rate was kept at 30  $\mu$ L/min (1.8 ml/h) in a relative humidity of 30-40%. After deposition, the fibers were transferred to an oven at 65°C for 10 minutes to remove traces of solvent. The resulting fibers were subjected to heat treatment in a muffled furnace (Nabertherm LH 15/12) for the combustion of the organic compounds in the air with a temperature slope of 1°C/min to 500°C for 8 hours and 40 minutes and then kept at 500°C for two hours. The resulting fibers are named 0.5Pd-ZNF, 1Pd-ZNF, and 2Pd-ZNF which corresponds to 0.5, 1, 2 % w/w of Pd in ZrO<sub>2</sub> for simplicity.

### 3.2 Morphological characterization

The scanning electron microscope images were taken by (HR)-SEM (Zeiss MERLIN SEM microscope) operated at 1.40 kV coupled with High-Efficiency Secondary Electron Detector (HE-SE2). Two milligrams of each sample were crushed in a mortar and placed on a carbon tape for an easier analysis by the SEM operator.

### 3.3 Spectroscopic characterization

The spectral data was gathered at different number of integration times either 5s x 60 or 1s x 100. A Nd:YAG 532 nm laser at 10 mW power was used as a photon source. The spectrometer (Alpha 300, WiTec) and the detector (Olympus MPlanFL N 10x / 0.3 Objective, 600 g mm<sup>1</sup> grating) calibrated on Si peaks.

### 3.4 Structure characterization

The crystal structure of the nanofibers was analyzed using XRD (D2 PHASER, Bruker) using a  $\text{CuK}\alpha$  source with a wavelength of (1.5406 Å) operated at 30 kV, 10mA, in the  $2\theta$  range between 20-80°, a step size of 0.05° and a scan speed of 0.1°/s. A Si low background sample holder (Bruker) as a sample substrate.

## 4 Results and discussion

### 4.1 X-ray Diffraction Spectroscopy

ZNF crystal structure is essential in analyzing its theoretical capabilities as a substrate material. Thus an X-ray diffraction spectroscopy is used to determine the phase and crystallite size of the nanofibers. Raw XRD data has been processed by removing the background (CrystalSleuth) and smoothed using Adjacent-Averaging with 5 points of window (OriginPro 2019). The resulting XRD diffractogram Fig.3 reveals three distinct diffraction patterns of the samples 0.5Pd-ZNF, 1Pd-ZNF, and 2Pd-ZNF, respectively, with  $2\theta$  angles between  $20^\circ$  and  $80^\circ$ . The main diffraction peak can be observed in all three samples fig.3 at  $30.3^\circ$ , corresponding to the tetragonal phase with lattice parameters (111). Multiple reflections at lower intensities can be observed at  $50.3^\circ$  (220) and  $60.16^\circ$  (311), both corresponding to the tetragonal phase (JCPDS-80-0965) [20]. However, there are also peaks corresponding to the monoclinic phase (JCPDS:37-1484) [20] at very low intensity. Mainly  $35.11^\circ$  (200), which is an overlapping peak with the tetragonal phase, also a soft peak at  $28.3^\circ$  (111) can be observed with an additional shoulder stretching into the main peak at  $31.6^\circ$  (111). The concentration of the monoclinic phase in the samples was found to be roughly 23% using an equation (1) proposed by Ulrich et al. [21].

Equation proposed by Ulrich[21]:

$$V_m = \frac{PX_m}{1-(P-1)X_m} \quad (1)$$

Where:

$$X_m = \frac{I_m^{(\bar{1}11)} + I_m^{(111)}}{I_m^{(\bar{1}11)} + I_m^{(111)} + I_t^{(101)}}$$

$P$  – correction factor of (1.34) accounting for lower density of the phases

$I_m^{(\bar{1}11)}$  – The intensity of the monoclinic peak at  $28.2^\circ(\bar{1}11)$ ;

$I_m^{(111)}$  – The intensity of the monoclinic peak at  $31.6^\circ(111)$ ;

$I_t^{(101)}$  – The intensity of the tetragonal peak at  $30.3^\circ(101)$ ;

Using Scherrer's equation (2) it is possible to determine the average Grain size size: Scherrer Equation:

$$D = \frac{K\lambda}{\beta 2 \cos(\theta)} \quad (2)$$

Average grain size of the zirconia crystals was determined to be 7.98 nm, 7.91 nm, 7.52nm for 0.5Pd-ZNF, 1Pd-ZNF and 2Pd-ZNF respectively. With a trend in decreasing grain size of tetragonal zirconia with increase in concentration of palladium.

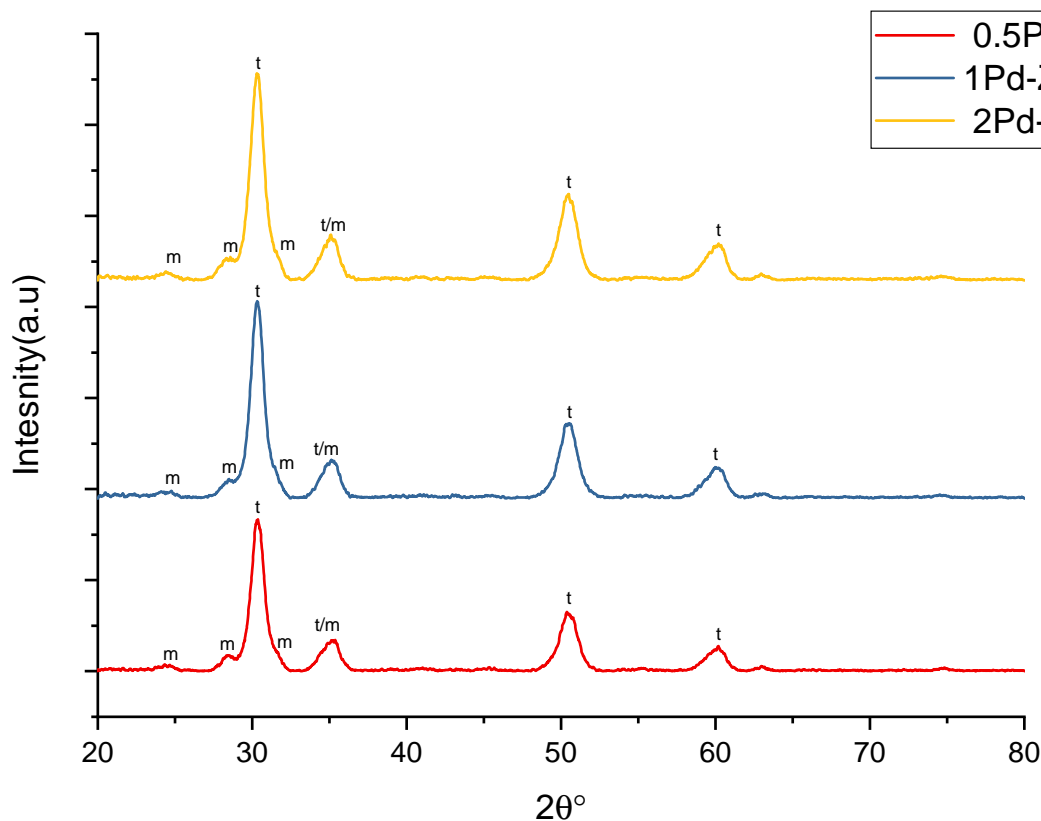


FIGURE 3: XRD diffraction patterns of nanofibers in powder form, with various Pd concentrations at 0.5% Pd, 1% Pd, and 2% Pd

Palladium oxide peaks cannot be evaluated due to close similarities with the zirconia structure. In figure.11, the main palladium oxide peak can be observed at  $34^\circ(200)$ , which has a high chance of being overpowered by the  $35.11^\circ(200)$  t/m broad peak. Because only 23% of zirconia is in the monoclinic phase, it can be concluded that most of the sample is tetragonal. An abundance of tetragonal zirconia phase is much more favorable for catalysis due to the porous structures it forms. The total surface area [22] of the tetragonal phase is higher than the monoclinic or cubic phase. A high surface area allows more access to the catalyst sites and is advantageous. On top of that small crystallite size of t-ZrO<sub>2</sub> has proved to offer high selectivity [23] towards isobutene in CO hydrogenation reactions.

## 4.2 Raman Spectroscopy

Raman spectroscopy is used to determine the chemical structure and phase of the nanofibers. It is complementary to XRD since it primarily serves as a confirmation of the XRD data for crystalline material. The data had its background and cosmic rays removed (CrystalSleuth). Due to the noise, it was decided to smooth the curves using Adjacent-Averaging with 5 points of window. Additionally, peak fitting was performed using Lorentz distribution (OriginPro 2019). The resulting spectrum fig.4 revealed broad peaks with a relatively low resolution, indicative of small grain size and an overall disorder in the crystal structure [24]. The spectra resulted in five distinct peaks in vibrational bands at 176, 330, 373, 470, and 627  $\text{cm}^{-1}$ . According to the literature, the resulting data is characteristic of the monoclinic phase in zirconium dioxide [20],[25] for all three samples. It should be noted that there is a shift in all the data points by approximately 4  $\text{cm}^{-1}$  due to the detector calibration. Some low eminences at very low intensity, mainly 143  $\text{cm}^{-1}$  and 256  $\text{cm}^{-1}$ , belong to the tetragonal phase [24], and a shoulder 500  $\text{cm}^{-1}$  that might result from peak 470  $\text{cm}^{-1}$  of the tetragonal phase and 504  $\text{cm}^{-1}$  of the monoclinic overlapping. The evidence that a tetragonal phase is present in the samples persists, although it contradicts the XRD data, a plausible scenario is that m-ZrO<sub>2</sub> and t-ZrO<sub>2</sub> are mixed. There are a few reasons why this might be the case. First, the relatively short penetration depth of the 532 nm laser (10 to 1.2  $\mu\text{m}$  [26]) resulted in the analysis of the surface fibers, which due to more exposure to heat in the oven, and poor overall heat conduction of the nanofibers, have resulted in a surface with a monoclinic phase. According to a research done on zirconia nanoparticles [27], it was found that the transition of the tetragonal to monoclinic phase takes place initially at the surface and can be determined only using a UV Raman due to its higher surface sensitivity.

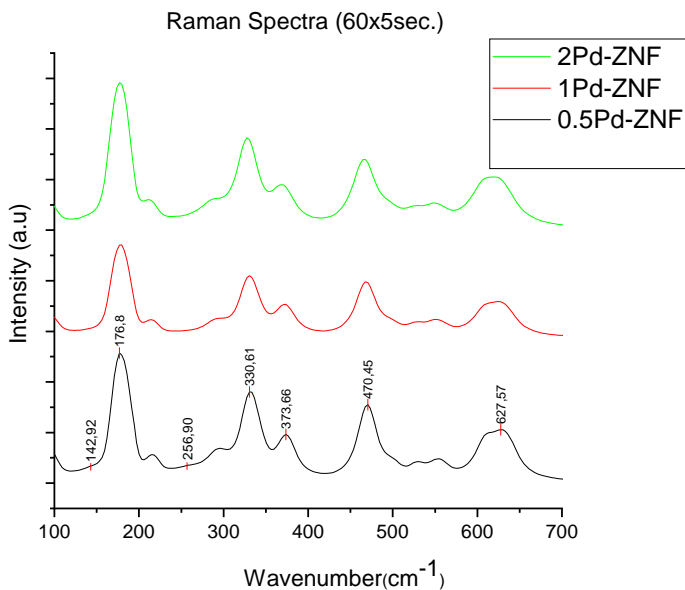


FIGURE 4: Raman spectra of ZNF's with various Pd concentrations at 0.5% Pd, 1% Pd, and 2% Pd, taken with 60 acquisitions at a 5 sec. integration time

### 4.3 X-ray photoelectron spectroscopy

The X-ray photoelectron spectrum is too complex for this thesis. Thus, it will not be studied in-depth, and all the supporting information can be found in the appendix. However, it gives a good insight into the surface of the fabricated nanofibers. The spectrum fig.9 was taken from the 2% sample since it has higher concentrations of components and has been found to contain Pd 337.5 eV in the 3d [28] electron configuration. The Pd3d configuration means that the palladium found on the surface is predominantly in its oxide form, PdO, which agrees with other research on palladium nanoparticles [9]. Peak intensity fig.9 suggests a low concentration of Pd on the fiber's surface, roughly 1.63%, meaning that the bulk of the palladium particles is likely to be buried inside the fibers.

A doublet found in the 180 eV to 188 eV is characteristic [29] to  $Zr3d_{5/2}$  and  $Zr3d_{3/2}$  respectively. This implies a valence of  $Zr^{+4}$  belonging to zirconium oxide. A high peak found at 284 eV fig.14 belonging to C1s suggests the presence of carbon [29], presumably from the combustion process of the polymer. Additionally, low-intensity peaks at 286, 287, and 289 eV prove the presence of carbonates. The broad O1s peak in figure.15 at 532 eV further reinforces the fact that carbonates are present that deconvoluted the peak. XPS has been able to provide valuable information on the 2Pd-ZNF sample. It proved that some of the precursor polymer had not been fully combusted, resulting in the low presence of different carbonates on the surface of the fibers. Additionally, besides EDS, it was able to determine if there is any palladium, mainly in its oxide form, which was proven to be much more active toward CO oxidation [9].

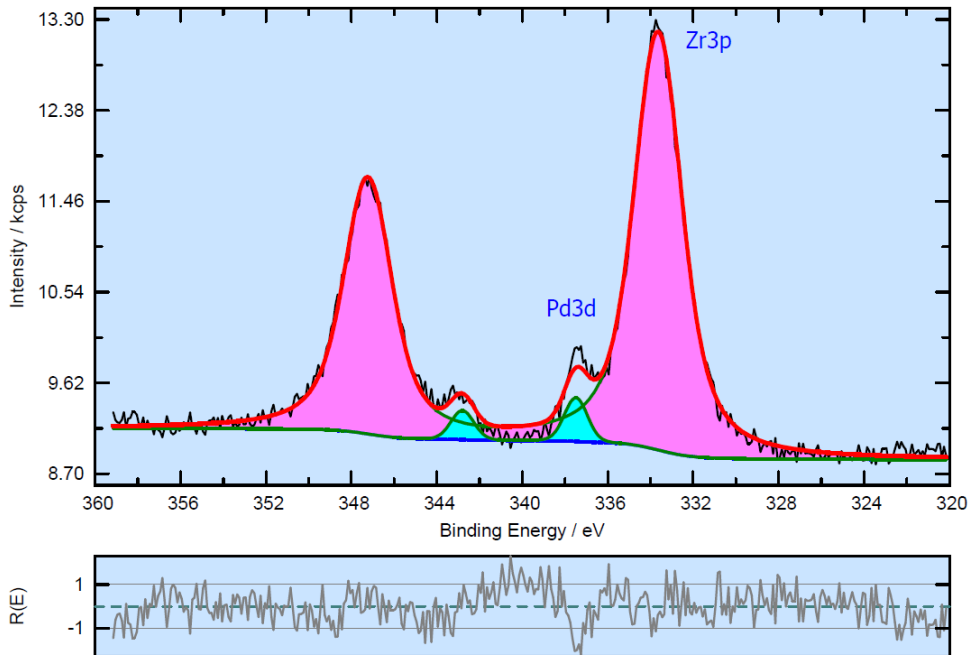


FIGURE 5: XPS spectrum of 2Pd-ZNF annealed at 500°C

## 4.4 Morphological analysis

SEM images of the zirconia nanofibers after annealing can be seen in fig.7(A)-(C), including the nanofibers before annealing in figure.6. Judging by the scans, all three  $\text{ZrO}_2$  fibers appear to be undamaged and free from any sintering with each other. The previous observation reinforces the results obtained from the XRD data that the bulk of the sample is in the tetragonal form of zirconia since, according to SEM data from other sources [5], the m- $\text{ZrO}_2$  fibers have a high degree of sintering and form zirconium beads instead of threads. However, some fibers exhibit a certain degree of roughness. In figure.12 (appendix), it can be seen that the surface fiber has different morphology than the fibers buried under it. Some surface fibers are likely to be in the monoclinic phase. This observation agrees with the Raman data, which further reinforces the theory that surface fibers are in a transition to the monoclinic phase. No Pd nanoparticles were observed on the surface of the nanofibers, possibly due to the low concentrations of the palladium but also the relatively large scale (200 nm) of the images.

A statistical image analysis was performed using an SEM image-analysis software (ImageJ) to estimate the average fiber diameter using a histogram from 40 measurements of individual threads in each image with eight bins. The histogram was fitted with a Gaussian distribution. Figure 8 is the resulting image analysis of the 0.5Pd-ZNF (A), 1Pd-ZNF (B), and 2Pd-ZNF (C) fibers with an average fiber diameter of  $56.15 \pm 1.03$  nm,  $51.12 \pm 0.65$  nm, and  $41.73 \pm 1.01$  nm, respectively. A decrease in fiber diameter following the addition of palladium has been observed. The prior observation agrees with the XRD data, where the increase in palladium concentration resulted in a smaller crystallite size, which also influenced the average fiber diameter.

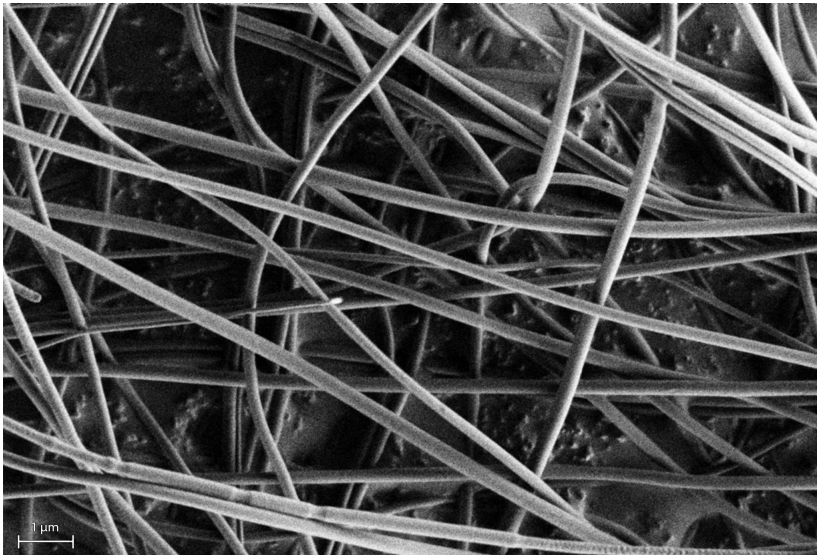
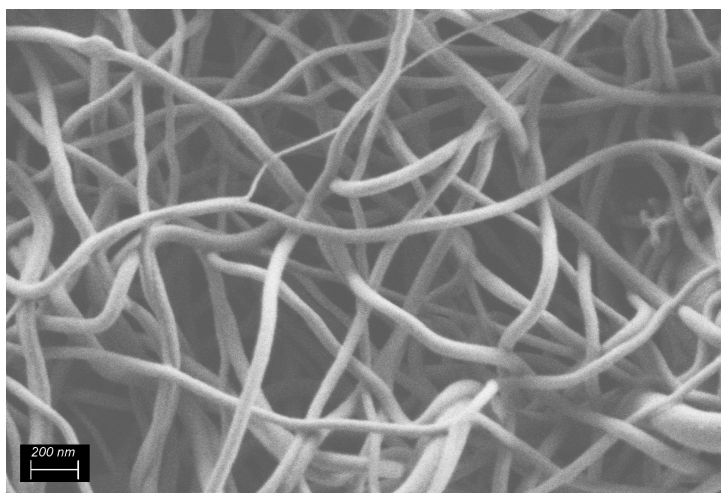
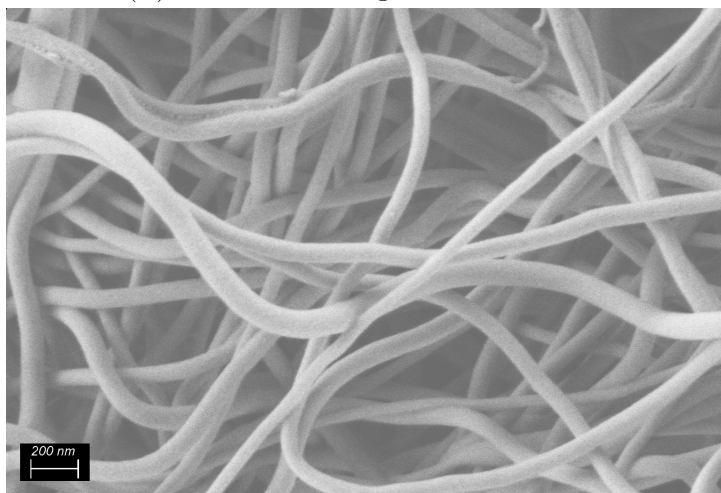


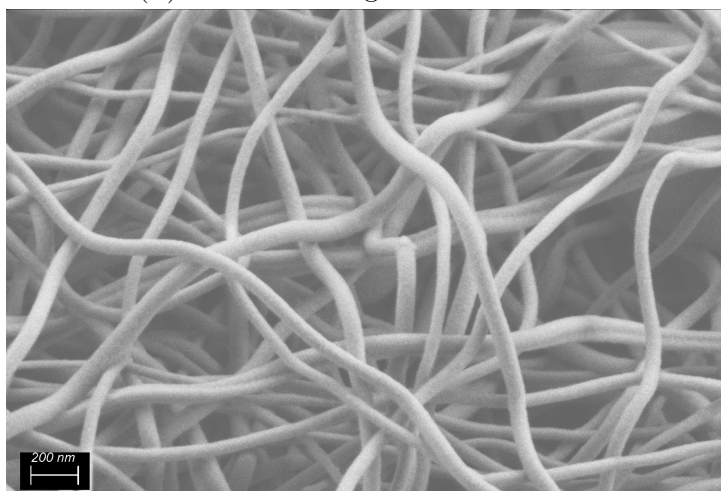
FIGURE 6: Nanofibers before annealing



(A) 0.5Pd-ZNF image at 200 nm scale

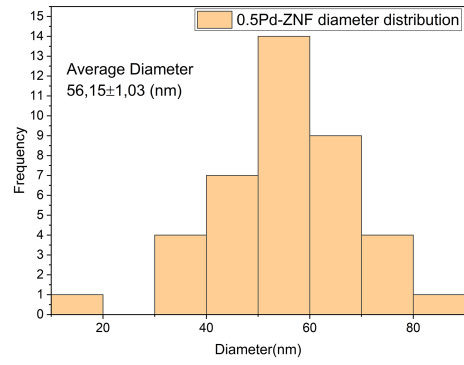
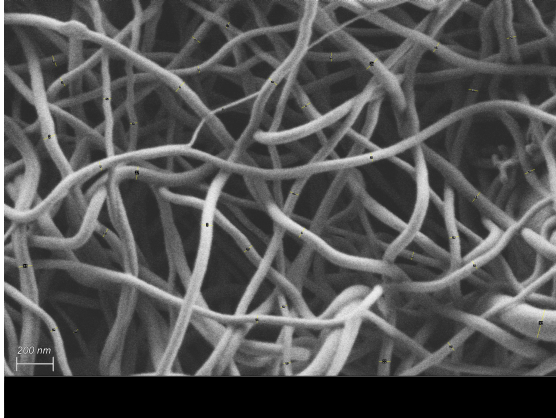


(B) 1Pd-ZNF image at 200 nm scale

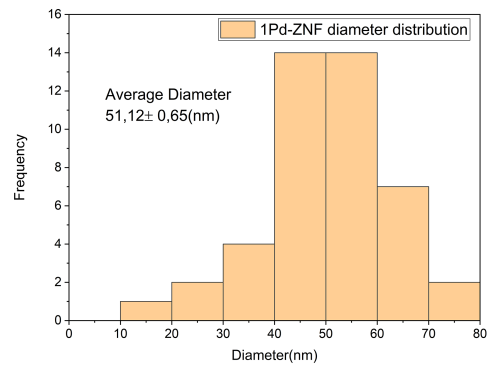
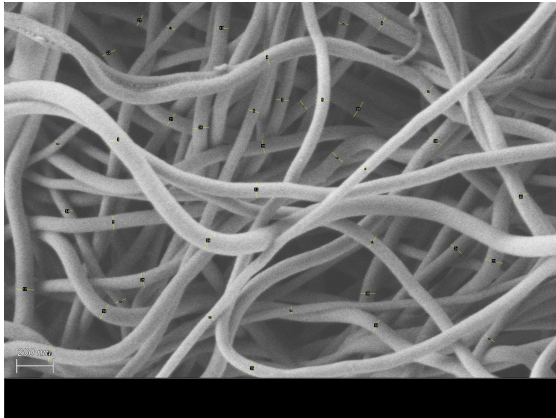


(C) 2Pd-ZNF image at 200 nm scale

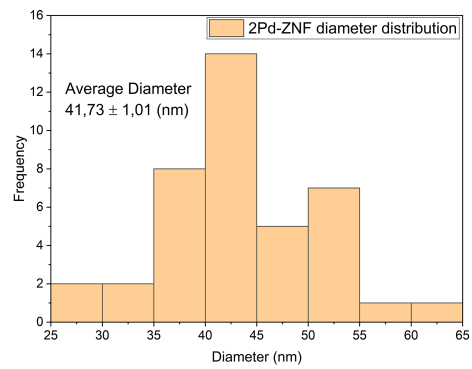
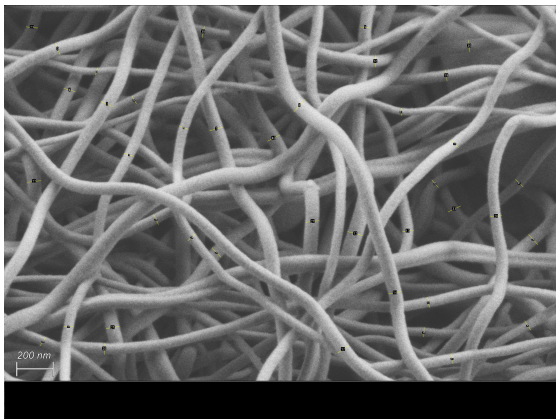
FIGURE 7: SEM images of a) 0.5% Pd, b) 1% Pd, c) 2% Pd nanofibers after calcination at 500°



(A) 0.5%Pd-ZNF fiber diameter distribution



(B) 1%Pd-ZNF fiber diameter distribution



(C) 2%Pd-ZNF fiber diameter distribution

FIGURE 8: Statistical analysis of average fiber diameter

#### 4.4.1 EDS (Energy-dispersive X-ray spectroscopy)

Parallel to SEM, EDS scans of all three samples were performed, as seen in figure.10 (c). From the images, it can be concluded that the 0.5Pd-ZNF fibers lack palladium. However, this occurs due to the interference of peaks in EDS data at low concentrations [30]. One and two percent samples, on the other hand, have palladium to weight ratio almost close to their intended concentration, 1.8 for 2% Pd and 0.9 for 1% Pd. The difference might be due to the standard error. A high carbon peak results from the carbon tape used to hold the samples in the SEM. It can also be seen from the mapping that the dispersity of palladium is not very uniform. Clumps of palladium particles are formed in the “beads” as a result of high precursor concentration in these regions during electrospinning. However, the resolution is so low that a quantitative analysis would be hard to perform. Non-other less, it serves as proof of the existence of palladium within the fiber. Traces of aluminum can be found in the 0.5Pd-ZNF’s, most likely its from the SEM chamber, as well as calcium which is most probably due to impurities in the palladium acetate.

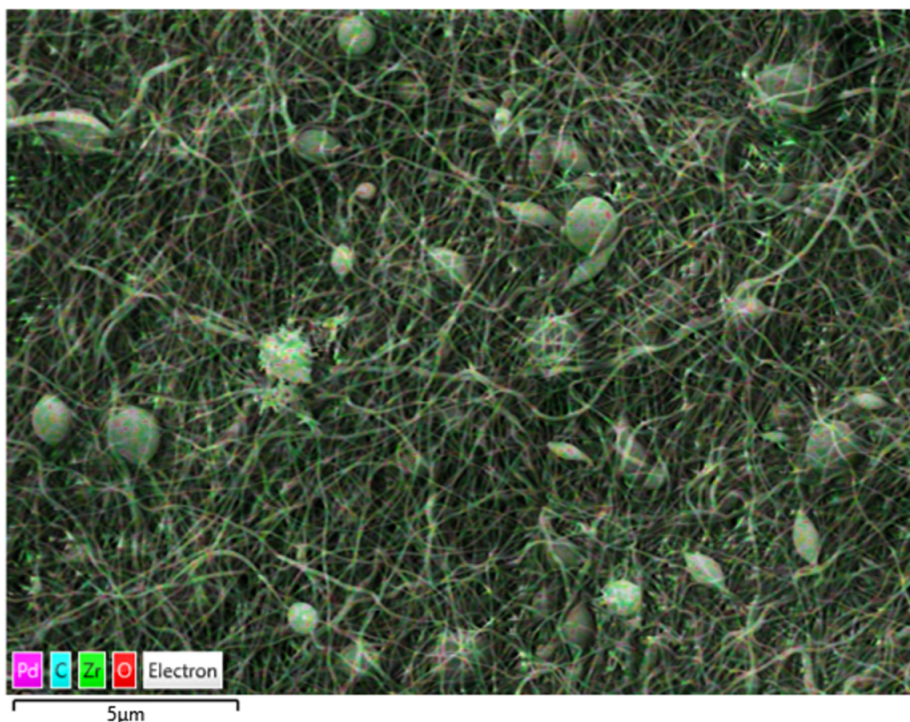
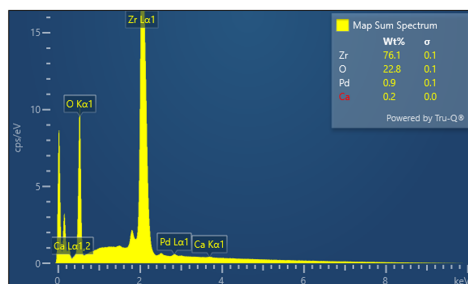
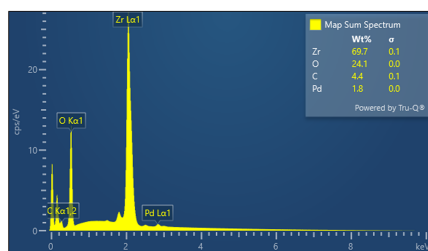


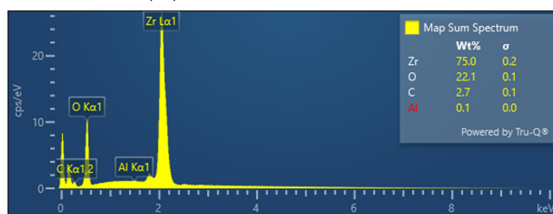
FIGURE 9: 2%Pd-ZNF EDS mapping



(A) 1% Pd-ZNF molecular composition



(B) 2% Pd-ZNF molecular composition



(C) 0.5% Pd-ZNF molecular composition

FIGURE 10: Chemical composition of the samples

## 5 Conclusions

Zirconium nanofibers functionalized with palladium nanoparticles were prepared using electrospinning. SEM analysis of the fibers revealed several discoveries, mainly smaller than 55 nm diameter of the fibers and a good consistency between its diameter dispersity. Low-diameter nanofibers will significantly influence the catalytic process since it results in a higher surface-to-volume ratio, facilitating the diffusion of gasses through mass transport. Both EDS and XPS confirmed the existence of palladium site's on the material's surface, possibly in its oxide form. XRD and Raman data, although contradictory, reveal the presence of two phases of  $\text{ZrO}_2$ , both monoclinic and tetragonal. However, a higher concentration of the tetragonal phase is more likely since both XRD and SEM give more evidence of the tetragonal phase. Mainly the characteristic fiber structure and the small crystallite size. A lot of evidence supports the correlation of Pd concentration with the diameter of the fibers. One of the main hypothesis is that palladium acetate influences the conductivity of the precursor solution, and as a result the Taylor cone formation, since the electrospinning was much more stable during the spinning of 2Pd-ZNFs. In-situ

preparation of zirconia nanofibers doped with palladium indeed yielded fibers with good characteristics for a support material, i.e, low diameter, mix of t and m phases, presence of palladium.

## **6 Acknowledgments**

I would like to thank Jędrzej Winczewski and Arturo Susarrey Arce for their help with the paper and for the enormous amount of feedback I got. Especially Jędrzej for helping out with all the measurements and training me to prepare the precursor solution, electrospin and the anneal the fibers. I would also like to thank Smithers Mark for operating the SEM and the acquisition of images.

## References

- [1] Palmisano G, Jitan SA, Garlisi C. 2022 Heterogeneous catalysis fundamentals, engineering and characterizations. *Heterogeneous Catalysis* pp. 1–25. (doi:10.1016/B978-0-323-89845-4.00001-1).
- [2] Guo Y, Wang X, Shen Y, Dong K, Shen L, Alzalab AAA. 2022 Research progress, models and simulation of electrospinning technology: a review. *Journal of Materials Science* **57**, 58–104. (doi:10.1007/S10853-021-06575-W).
- [3] Narayanan R, El-Sayed MA. 2003 Effect of catalysis on the stability of metallic nanoparticles: Suzuki reaction catalyzed by pvp-palladium nanoparticles. *Journal of the American Chemical Society* **125**, 8340–8347. (doi:10.1021/JA035044X/ASSET/IMAGES/LARGE/JA035044XF00004.JPEG).
- [4] Mondal K. 2017 Recent advances in the synthesis of metal oxide nanofibers and their environmental remediation applications. *Inventions 2017, Vol. 2, Page 9* **2**, 9. (doi:10.3390/INVENTIONS2020009).
- [5] 2019 Preparation of zirconia nanofibers by electrospinning and calcination with zirconium acetylacetonate as precursor. *Polymers 2019, Vol. 11, Page 1067* **11**, 1067. (doi:10.3390/POLYM11061067).
- [6] Chen Y, Lu W, Guo Y, Zhu Y, Lu H, Song Y. 2018 Synthesis, characterization and photocatalytic activity of nanocrystalline first transition-metal oxides nanofibers by electrospinning. *Applied Sciences 2019, Vol. 9, Page 8* **9**, 8. (doi:10.3390/APP9010008).
- [7] Xue J, Xie J, Liu W, Xia Y. 2017 Electrospun nanofibers: New concepts, materials, and applications. *Accounts of Chemical Research* **50**, 1976–1987. (doi:10.1021/ACS.ACCOUNTS.7B00218).
- [8] Angel M, Olguin R. 2022 Nanostructured (electro)catalysts with electrospinning (doi:10.3990/1.9789036553797).
- [9] Vedyagin AA, Volodin AM, Kenzhin RM, Chesnokov VV, Mishakov IV. 2016 Co oxidation over pd/zro2 catalysts: Role of supports donor sites. *Molecules 2016, Vol. 21, Page 1289* **21**, 1289. (doi:10.3390/MOLECULES21101289).
- [10] Mahata N, Vishwanathan V. 1999 Gas phase hydrogenation of phenol over supported palladium catalysts. *Catalysis Today* **49**, 65–69. (doi:10.1016/S0920-5861(98)00409-X).
- [11] Doshi J, Reneker DH. 1995 Electrospinning process and applications of electrospun fibers. *Journal of Electrostatics* **35**, 151–160. (doi:10.1016/0304-3886(95)00041-8).
- [12] Bonso JS, Kalaw GD, Ferraris JP. 2013 High surface area carbon nanofibers derived from electrospun pim-1 for energy storage applications. *Journal of Materials Chemistry A* **2**, 418–424. (doi:10.1039/C3TA13779A).

- [13] 1969 Electrically driven jets. *Proceedings of the Royal Society of London. A. Mathematical and Physical Sciences* **313**, 453–475. (doi:10.1098/RSPA.1969.0205).
- [14] Panda PK. 2007 Ceramic nanofibers by electrospinning technique-a review. *Transactions of the Indian Ceramic Society* **66**, 65–76. (doi:10.1080/0371750X.2007.11012252).
- [15] Verdoold S, Agostinho L, Yurteri C, Marijnissen J. 2014 A generic electrospray classification. *Journal of Aerosol Science* **67**, 87–103. (doi:https://doi.org/10.1016/j.jaerosci.2013.09.008).
- [16] Zhao YY, Yang QB, Lu XF, Wang C, Wei Y. 2005 Study on correlation of morphology of electrospun products of polyacrylamide with ultrahigh molecular weight. *Journal of Polymer Science Part B: Polymer Physics* **43**, 2190–2195. (doi:10.1002/POLB.20506).
- [17] Holzwarth U, Gibson N. 2011 The scherrer equation versus the 'debye-scherrer equation'. *Nature Nanotechnology 2011 6:9* **6**, 534–534. (doi:10.1038/nnano.2011.145).
- [18] Xu L, Wu XC, Zhu JJ. 2008 Green preparation and catalytic application of pd nanoparticles. *Nanotechnology* **19**, 305603. (doi:10.1088/0957-4484/19/30/305603).
- [19] Allen LJ, D'Alfonso AJ, Freitag B, Klenov DO. 2012 Chemical mapping at atomic resolution using energy-dispersive x-ray spectroscopy. *MRS Bulletin* **37**, 47–52. (doi:10.1557/MRS.2011.331).
- [20] Basahel SN, Ali TT, Mokhtar M, Narasimharao K. 2011 Influence of crystal structure of nanosized zirconia on photocatalytic degradation of methyl orange (doi:10.1186/s11671-015-0780-z).
- [21] Brossmann U, Würschum R, Södervall U, Schaefer HE. 1999 Oxygen diffusion in ultrafine grained monoclinic zro2. *Journal of Applied Physics* **85**, 7646. (doi:10.1063/1.370567).
- [22] Rodaev VV, Tyurin AI, Razlivalova SS, Korenkov VV, Golovin YI. 2021 Effect of zirconia nanofibers structure evolution on the hardness and young's modulus of their mats. *Polymers 2021, Vol. 13, Page 3932* **13**, 3932. (doi:10.3390/POLYM13223932).
- [23] Khaodee W, Jongsomjit B, Assabumrungrat S, Praserttham P, Goto S. 2007 Investigation of isosynthesis via co hydrogenation over zro2 and ceo2 catalysts: Effects of crystallite size, phase composition and acid–base sites. *Catalysis Communications* **8**, 548–556. (doi:10.1016/J.CATCOM.2006.08.001).
- [24] Ciszak C, Mermoux M, Gutierrez G, Leprêtre F, Duriez C, Popa I, Fayette L, Chevalier S. 2019 Raman spectra analysis of zro2 thermally grown on zircaloy substrates irradiated with heavy ion: Effects of oxygen isotopic substitution. *Journal of Raman Spectroscopy* **50**, 425–435. (doi:10.1002/JRS.5513).

- [25] Ding S, Zhao J, Yu Q. 2019 Effect of zirconia polymorph on vapor-phase ketonization of propionic acid. *Catalysts* **9**. (doi:10.3390/CATAL9090768).
- [26] Yi M, Zhang Y, Xu J, Deng D, Mao Z, Meng X, Shi X, Zhao B. 2021 Surface-enhanced raman scattering activity of zro2 nanoparticles: Effect of tetragonal and monoclinic phases. *Nanomaterials 2021, Vol. 11, Page 2162* **11**, 2162. (doi:10.3390/NANO11092162).
- [27] Li M, Feng Z, Xiong G, Ying P, Xin Q, Li C. 2001 Phase transformation in the surface region of zirconia detected by uv raman spectroscopy. *Journal of Physical Chemistry B* **105**, 8107–8111. (doi:10.1021/JP010526L).
- [28] Ding Y, Zhang L, Wu KH, Feng Z, Shi W, Gao Q, Zhang B, Su DS. 2016 The influence of carbon surface chemistry on supported palladium nanoparticles in heterogeneous reactions. *Journal of Colloid and Interface Science* **480**, 175–183. (doi:10.1016/j.jcis.2016.07.018).
- [29] Ruiz-Rosas R, Bedia J, Rosas JM, Lallave M, Loscertales IG, Rodríguez-Mirasol J, Cordero T. 2012 Methanol decomposition on electrospun zirconia nanofibers. *Catalysis Today* **187**, 77–87. (doi:10.1016/J.CATTOD.2011.10.031).
- [30] Ritchie NW, Newbury DE, Lowers H, Mengason M. 2018 Exploring the limits of eds microanalysis: rare earth element analyses. *IOP Conference Series: Materials Science and Engineering* **304**, 012013. (doi:10.1088/1757-899X/304/1/012013).
- [31] Muniz-Miranda M, Zoppi A, Muniz-Miranda F, Calisi N. 2020 Palladium oxide nanoparticles: Preparation, characterization and catalytic activity evaluation. *Coatings 2020, Vol. 10, Page 207* **10**, 207. (doi:10.3390/COATINGS10030207).

## A Abbreviations

NP	Nanoparticles
ZNF	Zirconium nanofibers
TCD	Nozzle to collector distance
XRD	X-ray diffraction spectroscopy
SEM	Scanning electron microscope
TEM	Transmission electron microscope
EDS	Energy dispersive X-ray spectroscopy
XPS	X-ray photoelectron spectroscopy
PVP	Polyvinylpyrrolidone

## B Palladium Oxide XRD

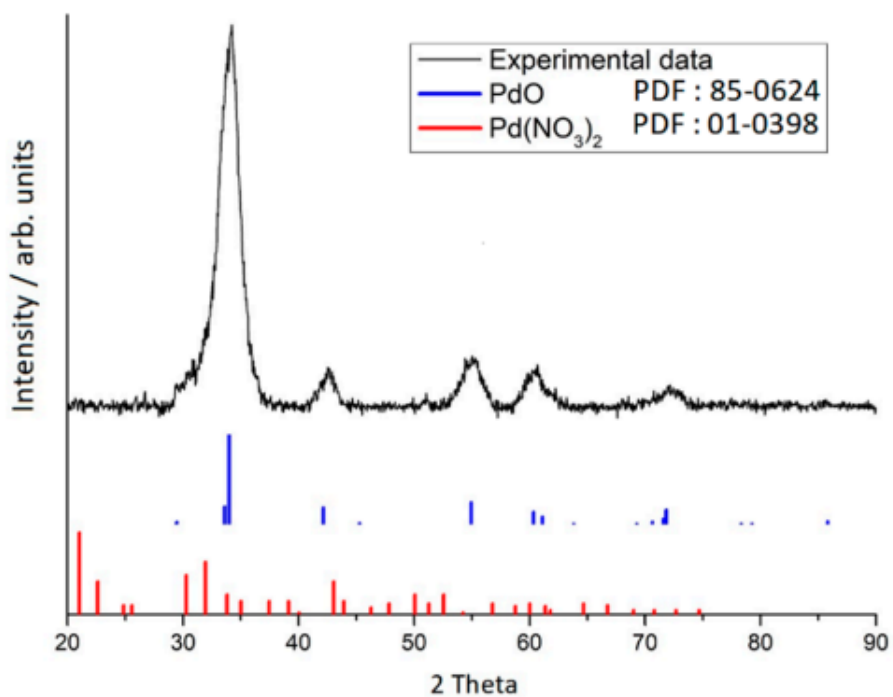


FIGURE 11: XRD data for palladium oxide, taken from [31]

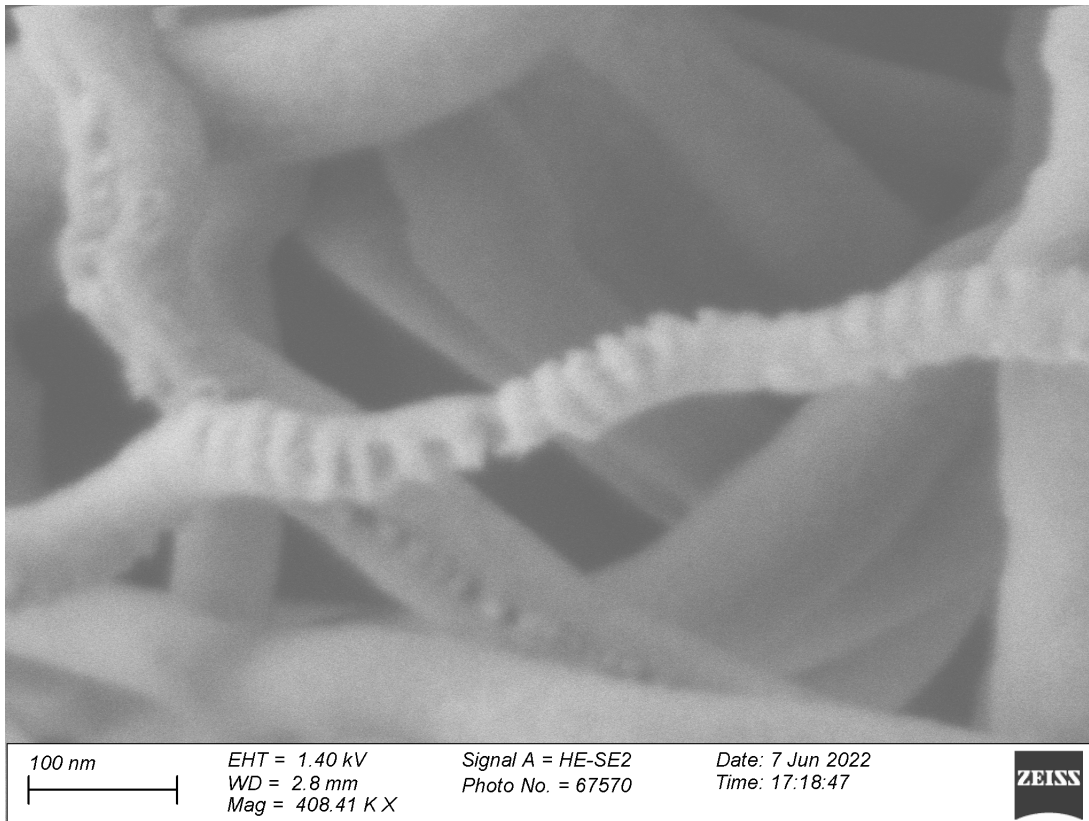


FIGURE 12: SEM image of zirconia nanofibers with monoclinic surface

C SEM

D XPS

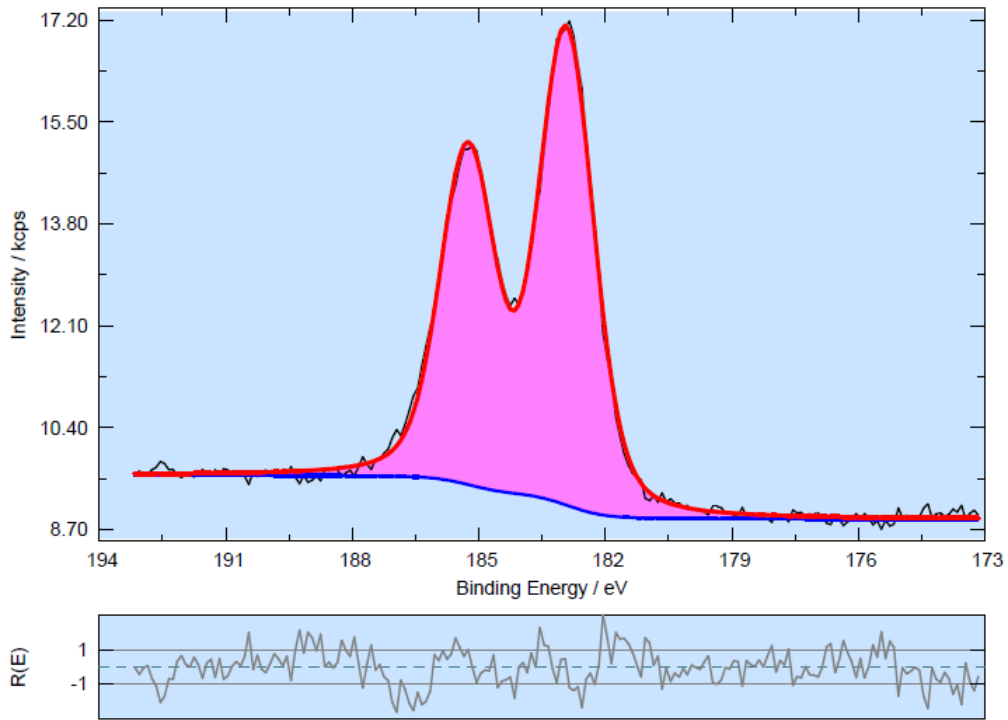


FIGURE 13: XPS spectra of Zr3d

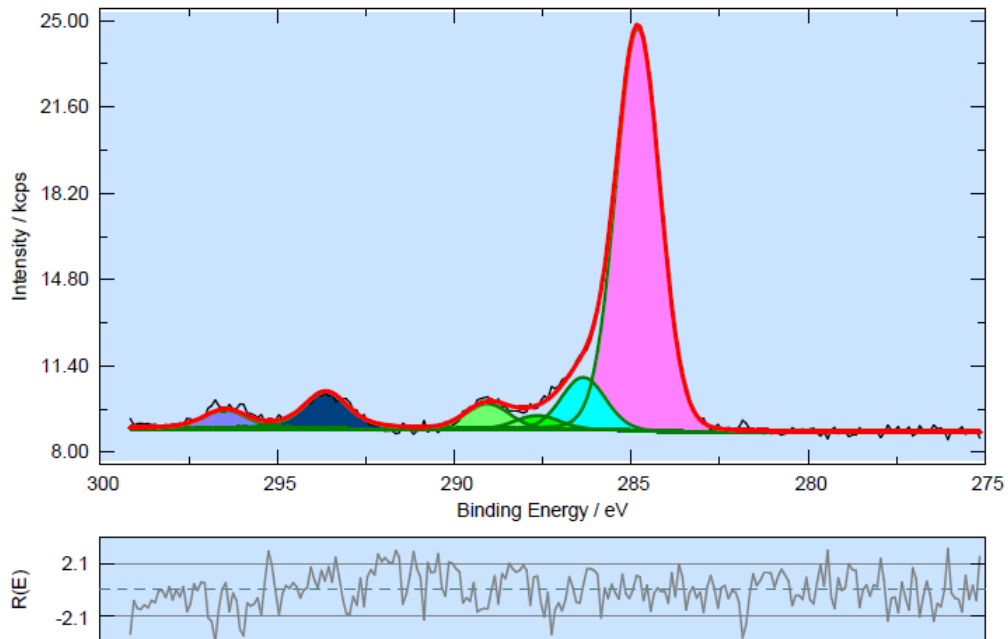


FIGURE 14: XPS spectra of C1s

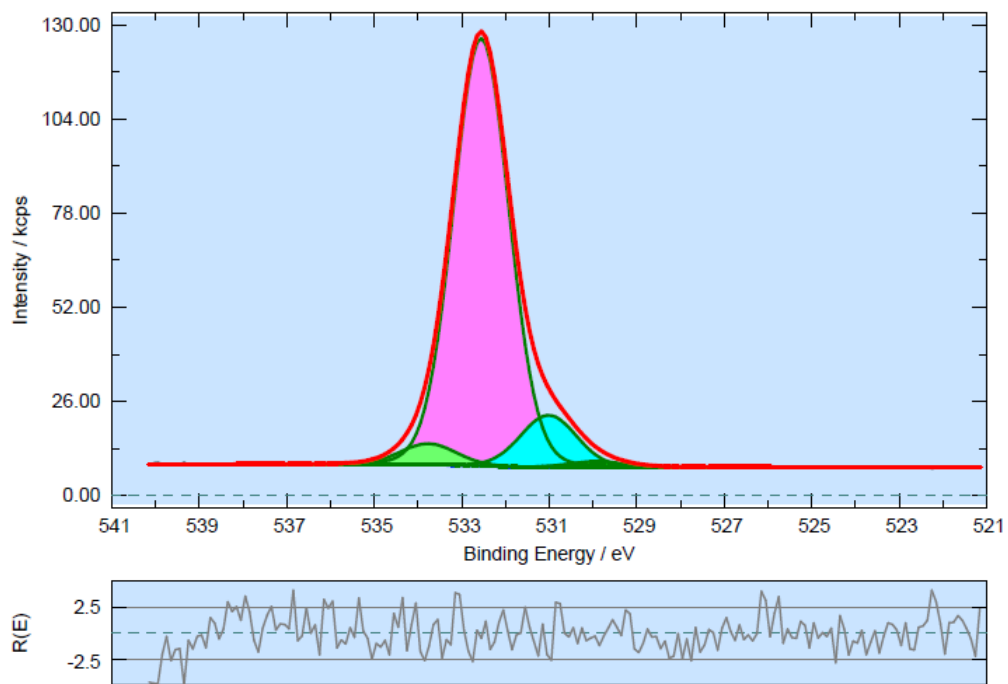


FIGURE 15: XPS spectra of O1s